JOURNAL OF AIRCRAFT
Vol. 48, No. 1, January–February 2011

Inverse Shape Design of Deformable Structures and Deformable Wings

Alejandro C. Limache*
International Center of Computational Methods in Engineering, 3000 Santa Fe, Argentina

DOI: 10.2514/1.C001007

Inverse methods are mathematical techniques by which the unknown input of a system is determined from a known or desired output. In this article, a new inverse method for the reverse design of deformable structures is presented. The inverse problem being addressed is the construction of the initial or unloaded shape of an structure such, when deformed under given loads, will acquire a desired predefined shape. The method can be used, among several other applications, for the inverse design of deformable airplane wings. For example, given a aerodynamically desired wing geometry, the method can be used to determine the real wing geometry that needs to be manufactured so that when such real wing deforms during flight under the influence of aerodynamic forces, it will naturally acquire the desired aerodynamic configuration. The presented inverse method is based on a novel and general approach which can be used with any structure made of hyperelastic materials. The inverse formulation is derived straightforwardly from the mathematical equations defining the standard direct approach of computational solid mechanics. On the computational side, this means that an inverse shape design code can be developed by making simple changes on an existing direct-analysis code.

I. Introduction

NOWADAYS, computational solid mechanics has become a fundamental tool in engineering design. Researchers work developing software that can predict numerically the behavior of solid materials under specific conditions. Using the software, engineers can in turn design structures or their components by studying their behavior, i.e., their deformation and stresses under work conditions. The vast majority of computational mechanics software is based on *direct methods* [1,2]. These type of methods provide solutions to the physical equations in the natural time-direction sense: given a known input to the system they determine its response. Numerical programs derived from these methods function as direct-analysis tools. When using such type of programs in structural design, a first trial for the geometry of the structure is suggested (for example with CAD) and the software is used to predict the deformation of the structure when subjected to given external loads. Then, based on the work of an expert the geometry of the structure is modified as many times as necessary until a desired behavior is obtained.

Usage of direct-analysis software reduces design costs since the different trial structures suggested during the design process do not need to be constructed, only the final design with the desired behavior is manufactured. In the wing design problem, for example, it would be extremely expensive to manufacture and test in a wind tunnel a wing geometry, to find out that the wing is useless because the structural deformation modifies the flow pattern affecting irreversibly the airplane's stability. Direct-analysis software helps to considerably reduce the design process since the wing can be modeled and then tested in a computer without the need to actually build it. Despite of its advantages the direct design approach is not perfect: it requires a continuous man-made modification of the wing's geometry in the computer until satisfactory results are obtained. Furthermore, there is not guarantee that the successive empirical modifications will lead to the desired objectives.

Received 13 March 2010; accepted for publication 6 May 2010. Copyright © 2010 by Alejandro C. Limache. Published by the American Institute of Aeronautics and Astronautics, Inc., with permission. Copies of this paper may be made for personal or internal use, on condition that the copier pay the $10.00 per-copy fee to the Copyright Clearance Center, Inc., 222 Rosewood Drive, Danvers, MA 01923; include the code 0021-8669/11 and $10.00 in correspondence with the CCC.

*Research Scientist of CONICET-INTEC, Guemes 3450; alejandrolimache@gmail.com.

Optimal Design is a successful methodology that removes the need of the successive man-made modifications required in the direct design. It is the computer who does that job. Optimal design methods work by finding an optimal design among a parameterized set of potential candidates using optimization techniques. Optimal design can be used to determine the best wing shape among a parameterized set of wings [3]. In this context, *the best* means the one that minimizes a cost function in which the desired properties are imposed. In optimal design still some human supervision may be necessary since there is not guarantee that just one given parameterized set will generate a global optimum with the required level of acceptable performance. Some references with aeronautical applications of optimal shape design are the following. Maruyama et al. [4] have designed tapered biplane wing to obtain better lift-to-drag ratio performances. Wu et al. [5] have developed an optimization tool for the design of fuselage shapes that yield a low-boom aircraft configuration. Barrett et al. [6] have presented a multifidelity search method to speed up airfoil shape design processes. In [7], three-dimensional aerodynamic surface optimization of blended wing bodies is carried out based on both continuous and discrete adjoint approaches. Lepine et al. [8] have worked on optimized aerodynamic wing design using nonuniform rational *B*-splines for the geometrical wing parameterization. In [9], using genetic algorithms, Ahn et al. have developed a method for optimal design of transonic wings with minimum drag and weight solving simultaneously for parameterized wing planforms and wing sections.

Aside from the direct methods and the optimal design techniques described above, there exists other class of design methods. These methods are called *inverse design methods*, or simply *inverse methods*. Inverse methods solve the reversed problem of a given system: given a specific output response of the system the inverse method determines what is the input that will make the system generate such specific output. Inverse methods also take the human out of the design loop with an additional advantage over the optimal design technique: they can find the exact match and not simply the best fit from a set. The applications of inverse methods are diverse. One area of application is the design of (high-lift) airfoils that generate specific pressure distributions [10,11]. Takanashi [12] has also developed an iterative three-dimensional inverse shape design method based on linear integro-differential equations of transonic flow. A review about trends in inverse shape design can be found in [13]. Inverse methods have been used also with success in the problem of structural health monitoring [14–16] where by reverse engineering the location and size of a fracture or damage on an

structure can be determined by collecting data of the vibration modes of the structure.

It must be pointed out that Inverse methods require that the associated mathematical equations leading to the reverse formulation be well-posed both theoretically and numerically and, as in the case of direct methods, they must contain the correct physical laws inside their formulation. As a consequence, a direct software can be (and should be) used to verify that, indeed, an inverse designed object truly generates the desired (output) response. Then, for the airfoil shape design problem cited above, any standard (Euler) flow code can be used to test that the designed airfoil truly generates the desired pressure distribution.

As a motivating example for the present article, let us consider now the problem of manufacturing a wing whose geometry is known to have ideal aerodynamic properties. If this ideal geometry is the one that is manufactured, once in flight, a structural problem appears: the weight and the strong aerodynamic forces will produce a deformation of the wing modifying its original shape. In turn, the resulting deformed shape will change the whole flow pattern, and as result, the wing will loose all of its known aerodynamic characteristics. To circumvent the problem, typically, a designer will need to remodel and test new unloaded wings until get one remodeled wing that after deformation will recover the desired aerodynamic characteristics. This is of course a extremely costly solution.

Instead, one would like to solve the following inverse problem: to determine exactly the wing's undeformed geometry that actually needs to be manufactured so that, in real flight, it will deform acquiring the aerodynamically desired configuration. This is the type of problem that the inverse method presented here can solve.

In general, the inverse design method presented in this article can be used to determine the undeformed shapes of elastic structures such when loaded will deform to prespecified target shapes.

Previous numerical models for the inverse design of hyperelastic bodies subjected to large deformations have been proposed by Govindjee and Mihalic [17,18], Yamada [19] and recently by Fachinotti et al. [20]. Except by Yamada's method, which is based on an arbitrary Lagrangian–Eulerian formulation, the models are based on an Eulerian formulation. To obtain the equations that solve the inverse problem, these methods require either to reformulate the equations of structural mechanics from the common Lagrangian setting to the less common Eulerian setting or to reformulate the standard constitutive equations of the equivalent direct problem. This posses a severe limitation to the generality of these methods because, for every constitutive law, work needs to be done for obtaining a reverse constitutive model. Furthermore, for large deformations, usually new stress and strain tensors need to be defined which are different from the standard Piola–Kirchhoff stresses and Green–Lagrange strains naturally used in direct-analysis programs. Also, as pointed out in [20], rewriting the constitutive equations complicates the description of orthotropic materials whose preferred directions are usually defined in the unknown undeformed configuration.

Instead, the method presented here is based on a pure Lagrangian formulation and consequently is based on the most natural point of view of computational solid mechanics. The presented formulation does not require a reformulation of the equilibrium equations neither to rewrite the constitutive equations. Furthermore, the same type of stress tensors and strain measures used in standard direct methods are employed, there is not need to add any additional ingredient. The method is based on general equations of continuum mechanics (so it can be applied to large deformation problems) and can be used with any family of hyperelastic constitutive equations. It can be used in problems dealing with large rotations and large deformations and satisfies objectivity.

As it will be seen, the presented inverse method exploits a duality concept between the deformed configuration and the initial configuration. Such, duality allows us to obtain an inverse formulation requiring the solution of nonlinear equations in a way identical to the direct method. Even more, the functional residue of the inverse method is exactly the same residue than the one used in the direct method. Only, a slightly different elemental Jacobian (tangent matrix) is required. The applications of the method are wide, particularly in manufacture processes of deformable structures [20]. As useful test examples, we will consider the problems of wing design and beam design.

The article is structured as follows. First, to more easily understand how the inverse method works, we will describe how numerical solutions of the direct method are obtained. For this purpose, the standard continuum mechanics framework is introduced, followed by a description of a typical finite element direct method. Finally, the inverse method will be built on top of the preexistent direct formulation. After the theory, numerical results obtained using the `MulPhys` code are shown. Such code was originally a solver of standard (direct) structural analysis problems, now, it can be used either as a standard direct-analysis tool or as inverse design tool.

II. Continuum Mechanics Framework

A. Undeformed and Deformed Configurations

Continuum mechanics provides the mathematical framework for the motion and deformation of material bodies. A material body $\mathcal{B}$, i.e., any structure, is formed by a continuous set of material particles $\mathfrak{p}$.

The body is defined by the specification of its configuration $\mathcal{B}^{\mathbf{0}}$, i.e., its geometry and its material properties, at a certain state (denoted here with the upper-index $\mathbf{0}$) when it is available for inspection. In this state, the body's geometry is defined in terms of a function $\bar{\boldsymbol{x}}^{\mathbf{0}}$ giving the vector position $\boldsymbol{x}^{\mathbf{0}}$ of each body's particle $\mathfrak{p}$ in space:

$$\boldsymbol{x}^{\mathbf{0}} = \bar{\boldsymbol{x}}^{\mathbf{0}}(\mathfrak{p}) \tag{1}$$

During inspection any required physical property can be obtained, for example, the body's density field $\rho^{\mathbf{0}}$

$$\rho^{\mathbf{0}} = \bar{\rho}^{\mathbf{0}}(\boldsymbol{x}^{\mathbf{0}}) \tag{2}$$

or the body's Cauchy tensor stress $\boldsymbol{\sigma}^{\mathbf{0}}$:

$$\boldsymbol{\sigma}^{\mathbf{0}} = \bar{\boldsymbol{\sigma}}(\boldsymbol{x}^{\mathbf{0}}) \tag{3}$$

Since inspection is selected to occur when the body is in the undeformed state not being subjected to any external forces, the configuration of specification, depicted in Fig. 1, is then called the *undeformed configuration*. By definition in the undeformed configuration the initial stress state is zero:

$$\boldsymbol{\sigma}^{\mathbf{0}} \equiv \mathbf{0} \tag{4}$$

The undeformed configuration is sometimes called *reference configuration* in the literature, however, for the sake of clarity we will not use such naming convention.

When external forces act on it, the body deforms changing its initial state $\mathcal{B}^{\mathbf{0}}$ to a new equilibrium state $\mathcal{B}^{\mathbf{1}}$, called *deformed configuration* and denoted here with the upper-index $\mathbf{1}$, as shown in Fig. 2. The deformed configuration is described in terms of new vector positions $\boldsymbol{x}^{\mathbf{1}}$ of the material particles in physical space

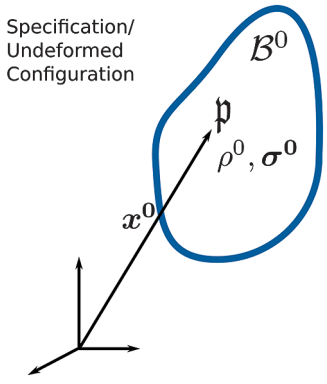


Fig. 1 Specification/undeformed configuration.

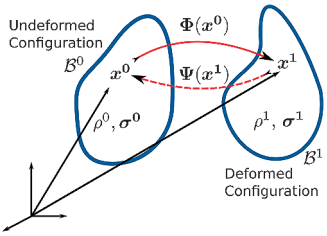


Fig. 2 Undeformed configuration and deformed configuration.

$$\boldsymbol{x}^{\mathbf{1}} = \bar{\boldsymbol{x}}^{\mathbf{1}}(\mathrm{p}) \tag{5}$$

Combination of Eqs. (1) and (5) allows to define the *deformation map* $\boldsymbol{\Phi}(\boldsymbol{x}^{\mathbf{0}})$ from the undeformed particle's positions $\boldsymbol{x}^{\mathbf{0}}$ to their deformed positions $\boldsymbol{x}^{\mathbf{1}}$:

$$\boldsymbol{x}^{\mathbf{1}} = \boldsymbol{\Phi}(\boldsymbol{x}^{\mathbf{0}}) = \bar{\boldsymbol{x}}^{\mathbf{1}}(\bar{\boldsymbol{x}}^{\mathbf{0}^{-1}}(\boldsymbol{x}^{\mathbf{0}})) \tag{6}$$

The inverse map can also be defined

$$\boldsymbol{x}^{\mathbf{0}} = \boldsymbol{\Psi}(\boldsymbol{x}^{\mathbf{1}}), \quad \text{where } \boldsymbol{\Psi} = \boldsymbol{\Phi}^{-1} \tag{7}$$

Both, the deformation map and the inverse map are shown Fig. 2. Following the adopted upper-indices convention, in the deformed configuration the volume occupied by the body is denoted by $v^{\mathbf{1}}$ and the density field and stress field are denoted by $\rho^{\mathbf{1}}$ and $\boldsymbol{\sigma}^{\mathbf{1}}$, respectively.

A measure of the geometrical deformation is provided through the *deformation gradient* tensor $\boldsymbol{F}^{\mathbf{1}}_{\mathbf{0}}$, which is defined as the gradient of the deformation map $\boldsymbol{\Phi}$ with respect to coordinates of the undeformed configuration:

$$\boldsymbol{F}^{\mathbf{1}}_{\mathbf{0}} = \frac{\partial \boldsymbol{x}^{\mathbf{1}}}{\partial \boldsymbol{x}^{\mathbf{0}}} = \frac{\partial \boldsymbol{\Phi}(\boldsymbol{x}^{\mathbf{0}})}{\partial \boldsymbol{x}^{\mathbf{0}}} \tag{8}$$

If we denote by $\nabla^{\mathbf{0}}$ to the nabla operator in the undeformed configuration, the deformation gradient can be written simply as

$$\boldsymbol{F}^{\mathbf{1}}_{\mathbf{0}} = \nabla^{\mathbf{0}} \boldsymbol{x}^{\mathbf{1}} \tag{9}$$

Note that the gradient $\boldsymbol{F}^{\mathbf{0}}_{\mathbf{1}}$ of the inverse map $\boldsymbol{\Psi}$ with respect to spatial coordinates in the deformed configuration is precisely the inverse of $\boldsymbol{F}^{\mathbf{1}}_{\mathbf{0}}$, that is to say:

$$\boldsymbol{F}^{\mathbf{0}}_{\mathbf{1}} = \frac{\partial \boldsymbol{x}^{\mathbf{0}}}{\partial \boldsymbol{x}^{\mathbf{1}}} = \left[\frac{\partial \boldsymbol{x}^{\mathbf{1}}}{\partial \boldsymbol{x}^{\mathbf{0}}}\right]^{-1} = [\boldsymbol{F}^{\mathbf{1}}_{\mathbf{0}}]^{-1} \tag{10}$$

B. Equilibrium Equations: Strong Form

The equations of conservation of mass and momentum balance define deformation and motion of material bodies. The equation of conservation of mass can be integrated exactly leading to the following relationship between density values

$$\rho^{\mathbf{1}} J^{\mathbf{1}}_{\mathbf{0}} = \rho^{\mathbf{0}} \tag{11}$$

where $J^{\mathbf{1}}_{\mathbf{0}}$ stands for the determinant of the deformation gradient

$$J^{\mathbf{1}}_{\mathbf{0}} = \det(\boldsymbol{F}^{\mathbf{1}}_{\mathbf{0}}) \tag{12}$$

The momentum balance equations, on the other hand, define the equilibrium conditions at the deformed configuration $\mathcal{B}^{\mathbf{1}}$,

$$\nabla^{\mathbf{1}} \cdot \boldsymbol{\sigma}^{\mathbf{1}} + \rho^{\mathbf{1}} \boldsymbol{b} = \mathbf{0} \quad \text{forall } \boldsymbol{x}^{\mathbf{1}} \in \mathcal{B}^{\mathbf{1}} \tag{13}$$

where $\nabla^{\mathbf{1}}$ denotes the nabla operator in the deformed configuration and $\boldsymbol{b}$ denotes the external body forces per unit of mass. On the body's surface $\partial\mathcal{B}^{\mathbf{1}}$ two types of boundary conditions can be applied, point fixations and imposed traction forces $\boldsymbol{t}$:

$$\boldsymbol{x}^{\mathbf{1}} = \boldsymbol{x}^{\mathrm{fix}} \quad \text{forall } \boldsymbol{x}^{\mathbf{1}} \in \partial_x \mathcal{B}^{\mathbf{1}} \tag{14}$$

$$\boldsymbol{\sigma}^{\mathbf{1}} \cdot \boldsymbol{n}^{\mathbf{1}} = \boldsymbol{t} \quad \text{forall } \boldsymbol{x}^{\mathbf{1}} \in \partial_t \mathcal{B}^{\mathbf{1}} \tag{15}$$

C. Equilibrium Equations: Weak Form

The discretized equations are usually derived from the weak form of Eq. (13), which can be written as:

$$\int_{\mathcal{B}^{\mathbf{1}}} \nabla^{\mathbf{1}} \boldsymbol{\eta}^{\mathbf{1}} : \boldsymbol{\sigma}^{\mathbf{1}} \, \mathrm{d}v^{\mathbf{1}} - \int_{\mathcal{B}^{\mathbf{1}}} \boldsymbol{\eta}^{\mathbf{1}} \cdot \rho^{\mathbf{1}} \boldsymbol{b} \, \mathrm{d}v^{\mathbf{1}} - \int_{\partial_t \mathcal{B}} \boldsymbol{\eta}^{\mathbf{1}} \cdot \boldsymbol{t} \, \mathrm{d}a^{\mathbf{1}} = 0 \tag{16}$$

for every admissible variation $\boldsymbol{\eta}^{\mathbf{1}}$.

D. Constitutive Equations

The equilibrium equations are complete only when the Cauchy stress $\boldsymbol{\sigma}^{\mathbf{1}}$ is linked to a deformation measure through a constitutive equation. The constitutive equation of a general hyperelastic material can be written as follows [21]:

$$\boldsymbol{S}^{\mathbf{1}}_{\mathbf{0}} = \frac{\partial \bar{w}(\boldsymbol{E}^{\mathbf{1}}_{\mathbf{0}})}{\partial \boldsymbol{E}^{\mathbf{1}}_{\mathbf{0}}} = \bar{\boldsymbol{S}}^{\mathbf{1}}_{\mathbf{0}}(\boldsymbol{E}^{\mathbf{1}}_{\mathbf{0}}) \tag{17}$$

where $\bar{w}$ is the strain-energy density function, $\boldsymbol{S}^{\mathbf{1}}_{\mathbf{0}}$ is the second Piola–Kirchhoff stress tensor defined and $\boldsymbol{E}^{\mathbf{1}}_{\mathbf{0}}$ is the Green–Lagrange strain tensor, which are defined, respectively, as

$$\boldsymbol{\sigma}^{\mathbf{1}} = \frac{1}{J^{\mathbf{1}}_{\mathbf{0}}} (\boldsymbol{F}^{\mathbf{1}}_{\mathbf{0}} \cdot \boldsymbol{S}^{\mathbf{1}}_{\mathbf{0}} \cdot \boldsymbol{F}^{\mathbf{1}^T}_{\mathbf{0}}) \tag{18}$$

$$\boldsymbol{E}^{\mathbf{1}}_{\mathbf{0}} = \frac{1}{2} (\boldsymbol{F}^{\mathbf{1}^T}_{\mathbf{0}} \cdot \boldsymbol{F}^{\mathbf{1}}_{\mathbf{0}} - \boldsymbol{I}) \tag{19}$$

with $\boldsymbol{I}$ denoting the second-order identity tensor.

The most important point to be noted here is that, because of Eqs. (17–19), for hyperelastic materials, the Cauchy stress tensor can be computed as a unique function $\bar{\boldsymbol{\sigma}}^{\mathbf{1}}$ of the deformation gradient, that is to say, in general we can assume that

$$\boldsymbol{\sigma}^{\mathbf{1}} = \bar{\boldsymbol{\sigma}}^{\mathbf{1}}(\boldsymbol{F}^{\mathbf{1}}_{\mathbf{0}}) \tag{20}$$

Note that the employed formulation is general not been limited to linear-elasticity theory [22].

III. Finite Element Method Formulation

A. Spatial Discretization: Galerkin Approach

In the standard direct method, the body's undeformed geometry $\mathcal{B}^{\mathbf{0}}$ is known and the problem consists in finding the body's deformed geometry $\mathcal{B}^{\mathbf{1}}$ when given loads and body forces act on it. To solve the problem, both, the body and the equilibrium equations are discretized and solved numerically by the computer. In the present article, the finite element method will be used as the solution algorithm. The initial geometry $\mathcal{B}^{\mathbf{0}}$ is discretized in terms of a mesh $\mathcal{B}^{\mathbf{0}}_h$ formed by the union of (tetrahedral) elements $\Omega^{\mathbf{0}(e)}$. The mesh $\mathcal{B}^{\mathbf{0}}_h$ is defined through the vector position of its nodes and their element connectivities. We will denote by $\hat{\boldsymbol{x}}^{\mathbf{0}}$ to the global array containing the position coordinates of the n nodes of the mesh in the undeformed configuration

$$\hat{\boldsymbol{x}}^{\mathbf{0}} = \begin{bmatrix} \boldsymbol{x}^{\mathbf{0}}_1 \\ \vdots \\ \boldsymbol{x}^{\mathbf{0}}_\alpha \\ \vdots \\ \boldsymbol{x}^{\mathbf{0}}_n \end{bmatrix} \tag{21}$$

When subjected to external loads and body forces, the undeformed body or structure $\mathcal{B}^{\mathbf{0}}_h$ deforms to a deformed configuration $\mathcal{B}^{\mathbf{1}}_h$ defined by the union of the deformed (tetrahedral) elements $\Omega^{\mathbf{1}}_e$, which result from the mapping of undeformed nodal positions $\hat{\boldsymbol{x}}^{\mathbf{0}}$ into deformed

nodal positions $\hat{\boldsymbol{x}}^{\mathbf{1}}$. The direct problem consists in determining the location of the deformed n nodal positions $\hat{\boldsymbol{x}}^{\mathbf{1}}$

$$\hat{\boldsymbol{x}}^{\mathbf{1}} = \begin{bmatrix} \boldsymbol{x}_1^{\mathbf{1}} \\ \vdots \\ \boldsymbol{x}_\alpha^{\mathbf{1}} \\ \vdots \\ \boldsymbol{x}_n^{\mathbf{1}} \end{bmatrix} \tag{22}$$

defining the deformed body $\mathcal{B}_h^{\mathbf{1}}$.

The discrete equations that determine the deformed nodal positions $\hat{\boldsymbol{x}}^{\mathbf{1}}$ are obtained by restricting the admissible vector functions $\boldsymbol{\eta}^{\mathbf{1}}$ in Eq. (16) to a n-dimensional basis of weight/shape functions $N_\alpha = \bar{N}_\alpha(\boldsymbol{x}^{\mathbf{1}})$ where N_α is the shape function defined around the αth-node located at the position $\boldsymbol{x}_\alpha^{\mathbf{1}}$. Then, defining the n-dimensional vector array $\boldsymbol{N}$ containing the set of shape functions N_α, a standard variational procedure leads to the discrete equilibrium equations that must be satisfied at the deformed configuration:

$$\mathbf{R} = \int_{\mathcal{B}_h^{\mathbf{1}}} \nabla^{\mathbf{1}} \boldsymbol{N} \cdot [\boldsymbol{\sigma}^{\mathbf{1}}]^T \, \mathrm{d}v^{\mathbf{1}} - \int_{\mathcal{B}_h^{\mathbf{1}}} \boldsymbol{N} \rho^{\mathbf{1}} \boldsymbol{b} \, \mathrm{d}v^{\mathbf{1}} - \int_{\partial_t \mathcal{B}_h^{\mathbf{1}}} \boldsymbol{N} \boldsymbol{t} \, \mathrm{d}a^{\mathbf{1}} = \mathbf{0} \tag{23}$$

In the finite element method (FEM), all variables including the shape functions are defined elementwise. Then, given an element e, the upper-index (e) will be used to denote the restriction of any given variable to such element. For example, $\boldsymbol{N}^{(e)}$ will refer to the values of the shape function vector $\boldsymbol{N}$ in element e and $\hat{\boldsymbol{x}}^{\mathbf{1}(e)}$ will refer to the subset of deformed nodal positions $\hat{\boldsymbol{x}}^{\mathbf{1}}$ that form such element. For the case of (linear) tetrahedral elements such subset is formed by the four nodal positions that define the vertices of the tetrahedron e.

Using these elementwise definitions, in FEM, the residual vector function $\mathbf{R}$ given in Eq. (23) is computed by assembling the elemental residual $\mathbf{R}^{(e)}$ contributions of each element so that

$$\mathbf{R} = \sum_e [\mathbf{R}^{(e)}] \tag{24}$$

$$= \sum_e \left[\int_{\Omega^{\mathbf{1}(e)}} \nabla^{\mathbf{1}(e)} \mathbf{N}^{(e)} \cdot [\boldsymbol{\sigma}^{\mathbf{1}(e)}]^T \, \mathrm{d}v^{\mathbf{1}(e)} - \int_{\Omega^{\mathbf{1}(e)}} \boldsymbol{N}^{(e)} \rho^{\mathbf{1}(e)} \boldsymbol{b} \, \mathrm{d}v^{\mathbf{1}(e)} - \int_{\partial_t \Omega^{\mathbf{1}(e)}} \boldsymbol{N}^{(e)} \boldsymbol{t} \, \mathrm{d}a^{\mathbf{1}(e)} \right] \tag{25}$$

Using the isoparametric approach [23], both the interpolating functions $\boldsymbol{N}^{(e)}$ and the geometry of all elements $\Omega^{\mathbf{1}(e)}$ are defined in terms of the interpolating functions $\boldsymbol{N}^{\mathrm{ref}}$ associated with a reference or master element Ω^{ref} having local coordinates $\boldsymbol{\xi}^{\mathrm{ref}}$. Therefore, we have that

$$\boldsymbol{N}^{(e)} = \boldsymbol{N}^{\mathrm{ref}}(\boldsymbol{\xi}^{\mathrm{ref}}) \tag{26}$$

and

$$\boldsymbol{x}^{\mathbf{1}(e)} = \boldsymbol{N}^{\mathrm{ref}}(\boldsymbol{\xi}^{\mathrm{ref}}) \cdot \hat{\boldsymbol{x}}^{\mathbf{1}(e)} \tag{27}$$

Equation (27) defines the *isoparametric map* from the reference element domain Ω^{ref} to the deformed domain $\Omega^{\mathbf{1}(e)}$ of element e. Then, we can compute the deformation gradient $\boldsymbol{F}_{\mathrm{ref}}^{\mathbf{1}(e)}$ and the determinant of this map:

$$\boldsymbol{F}_{\mathrm{ref}}^{\mathbf{1}(e)} = \left[\frac{\partial \boldsymbol{x}^{\mathbf{1}(e)}}{\partial \boldsymbol{\xi}^{\mathrm{ref}}} \right] = \left[\frac{\partial \boldsymbol{N}^{\mathrm{ref}} \cdot \hat{\boldsymbol{x}}^{\mathbf{1}(e)}}{\partial \boldsymbol{\xi}^{\mathrm{ref}}} \right] = [\hat{\boldsymbol{x}}^{\mathbf{1}(e)}]^T \cdot \left[\frac{\partial \boldsymbol{N}^{\mathrm{ref}}}{\partial \boldsymbol{\xi}^{\mathrm{ref}}} \right] \tag{28}$$

$$J_{\mathrm{ref}}^{\mathbf{1}(e)} = \det(\boldsymbol{F}_{\mathrm{ref}}^{\mathbf{1}(e)}) \tag{29}$$

and transform integrals in deformed elements to integrals in the reference element. Performing this transformation in Eq. (25), we get that the residual function can be computed as an assembly of integrals in the master element:

$$\mathbf{R} = \sum_e \left[\int_{\Omega^{\mathrm{ref}}} \nabla^{\mathbf{1}(e)} \boldsymbol{N}^{\mathrm{ref}} \cdot [\boldsymbol{\sigma}^{\mathbf{1}(e)}]^T J_{\mathrm{ref}}^{\mathbf{1}(e)} \, \mathrm{d}v^{\mathrm{ref}} - \int_{\Omega_{\mathrm{ref}}} \boldsymbol{N}^{\mathrm{ref}} \rho^{\mathbf{1}(e)} \boldsymbol{b} J_{\mathrm{ref}}^{\mathbf{1}(e)} \, \mathrm{d}v^{\mathrm{ref}} \right] - \sum_e \left[\int_{\partial_t \Omega^{\mathrm{ref}}} \boldsymbol{N}^{\mathrm{ref}} \boldsymbol{t} J_{\mathrm{ref}}^{\mathbf{1}(e)} \parallel \boldsymbol{F}_{\mathrm{ref}}^{\mathbf{1}(e)-T} \cdot \boldsymbol{n}_{\mathrm{ref}} \parallel \mathrm{d}a^{\mathrm{ref}} \right] \tag{30}$$

In Eq. (30), $\boldsymbol{n}_{\mathrm{ref}}$ is the boundary unit normal of the reference element and where $\| \cdot \|$ is the standard vector magnitude.

Now, note that the gradient of the shape function $\nabla^{\mathbf{1}(e)} \boldsymbol{N}^{\mathrm{ref}}$ in any element e can be computed in terms of the gradient in the reference element, as follows:

$$\nabla^{\mathbf{1}(e)} \boldsymbol{N}^{\mathrm{ref}} = \frac{\partial \boldsymbol{N}^{\mathrm{ref}}}{\partial \boldsymbol{x}^{\mathbf{1}(e)}} = \frac{\partial \boldsymbol{N}^{\mathrm{ref}}}{\partial \boldsymbol{\xi}^{\mathrm{ref}}} \cdot \frac{\partial \boldsymbol{\xi}^{\mathrm{ref}}}{\partial \boldsymbol{x}^{\mathbf{1}(e)}} = \frac{\partial \boldsymbol{N}^{\mathrm{ref}}}{\partial \boldsymbol{\xi}^{\mathrm{ref}}} \cdot [\boldsymbol{F}_{\mathrm{ref}}^{\mathbf{1}(e)}]^{-1} \tag{31}$$

Using Eq. (31) and eliminating the deformed density $\rho^{\mathbf{1}}$, in terms of the known undeformed density $\rho^{\mathbf{0}}$ by means of Eq. (11), we get that:

$$\mathbf{R} = \sum_e \left[\int_{\Omega^{\mathrm{ref}}} \frac{\partial \boldsymbol{N}^{\mathrm{ref}}}{\partial \boldsymbol{\xi}^{\mathrm{ref}}} \cdot [\boldsymbol{F}_{\mathrm{ref}}^{\mathbf{1}(e)}]^{-1} \cdot [\boldsymbol{\sigma}^{\mathbf{1}(e)}]^T J_{\mathrm{ref}}^{\mathbf{1}(e)} \, \mathrm{d}v^{\mathrm{ref}} - \int_{\Omega_{\mathrm{ref}}} \boldsymbol{N}^{\mathrm{ref}} \rho^{\mathbf{0}(e)} \boldsymbol{b} J_{\mathrm{ref}}^{\mathbf{1}(e)} / J_{\mathbf{0}}^{\mathbf{1}(e)} \, \mathrm{d}v^{\mathrm{ref}} \right] - \sum_e \left[\int_{\partial_t \Omega^{\mathrm{ref}}} \boldsymbol{N}^{\mathrm{ref}} \boldsymbol{t} J_{\mathrm{ref}}^{\mathbf{1}(e)} \parallel \boldsymbol{F}_{\mathrm{ref}}^{\mathbf{1}(e)-T} \cdot \boldsymbol{n}_{\mathrm{ref}} \parallel \mathrm{d}a^{\mathrm{ref}} \right] \tag{32}$$

Observation 1: All quantities in the integrands of Eq. (32) are explicit functions of the deformation gradient $\boldsymbol{F}_{\mathrm{ref}}^{\mathbf{1}(e)}$. For example, that $\boldsymbol{\sigma}^{\mathbf{1}(e)}$ is a function of $\boldsymbol{F}_{\mathrm{ref}}^{\mathbf{1}(e)}$ follows from the fact that $\boldsymbol{\sigma}^{\mathbf{1}}$ is a function of the deformation gradient $\boldsymbol{F}_{\mathbf{0}}^{\mathbf{1}}$ [see Eq. (20)], and that, in turn, such deformation gradient can be written in terms of $\boldsymbol{F}_{\mathrm{ref}}^{\mathbf{1}}$ as:

$$[\boldsymbol{F}_{\mathbf{0}}^{\mathbf{1}}] = [\boldsymbol{F}_{\mathrm{ref}}^{\mathbf{1}}] \cdot [\boldsymbol{F}_{\mathbf{0}}^{\mathrm{ref}}] = [\boldsymbol{F}_{\mathrm{ref}}^{\mathbf{1}}] \cdot [\boldsymbol{F}_{\mathrm{ref}}^{\mathbf{0}}]^{-1} \tag{33}$$

Therefore, we can actually rewrite Eq. (20) for each element e as

$$\boldsymbol{\sigma}^{\mathbf{1}(e)} = \bar{\boldsymbol{\sigma}}^{\mathbf{1}}([\boldsymbol{F}_{\mathrm{ref}}^{\mathbf{1}(e)}] \cdot [\boldsymbol{F}_{\mathrm{ref}}^{\mathbf{0}(e)}]^{-1}) \tag{34}$$

Similarly, $J_{\mathbf{0}}^{\mathbf{1}(e)}$ is also a function of $\boldsymbol{F}_{\mathrm{ref}}^{\mathbf{1}(e)}$ as can be seen by combining Eqs. (12) and (33):

$$J_{\mathbf{0}}^{\mathbf{1}} = J_{\mathrm{ref}}^{\mathbf{1}} J_{\mathbf{0}}^{\mathrm{ref}} = J_{\mathrm{ref}}^{\mathbf{1}} / J_{\mathrm{ref}}^{\mathbf{0}} \tag{35}$$

and Eq. (29).

Observation 2: Because each elemental deformation gradient $\boldsymbol{F}_{\mathrm{ref}}^{\mathbf{1}(e)}$ is an explicit function of $\hat{\boldsymbol{x}}^{\mathbf{1}(e)}$ by Eq. (28), all the elemental deformation gradients $\boldsymbol{F}_{\mathrm{ref}}^{\mathbf{1}(e)}$ are, ultimately, functions of the state of deformed positions $\hat{\boldsymbol{x}}^{\mathbf{1}}$.

Observation 3: All quantities in the integrands of Eq. (32) are, lastly, functions of the state of deformed positions $\hat{\boldsymbol{x}}^{\mathbf{1}}$. This follows straightforwardly from observations 1 and 2.

From observation 3, it is clear then that the residue $\mathbf{R}$ defined in Eq. (32) is a function of the vector $\hat{\boldsymbol{x}}^{\mathbf{1}}$ of deformed nodal variables, so we can write

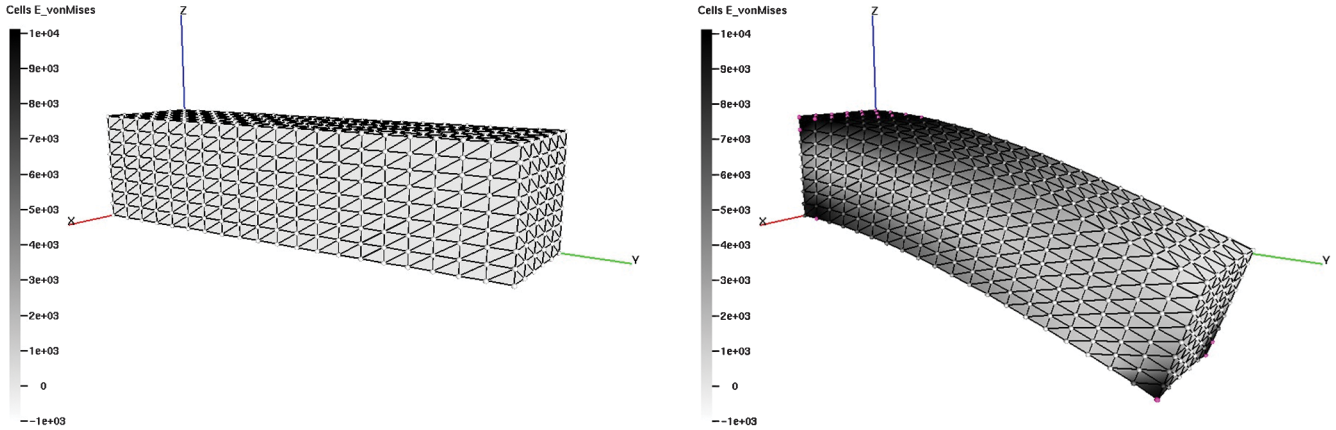
$$\mathbf{R} = \mathbf{R}(\hat{\boldsymbol{x}}^{\mathbf{1}}) \tag{36}$$

Now, a fundamental observation comes which will be the key for understanding the inverse method presented shortly.

Observation 4: The residual function Eq. (32) is actually not only a function of the deformed nodal coordinates $\hat{\boldsymbol{x}}^{\mathbf{1}}$ but also a function of the undeformed nodal coordinates $\hat{\boldsymbol{x}}^{\mathbf{0}}$. That is to say, the residue is a dual function:

$$\mathbf{R} = \mathbf{R}(\hat{\boldsymbol{x}}^{\mathbf{1}}; \hat{\boldsymbol{x}}^{\mathbf{0}}) \tag{37}$$

That the residual function can indeed be represented as in Eq. (37), follows from the fact that to evaluate the Cauchy stress $\boldsymbol{\sigma}^{\mathbf{1}(e)}$



a) [Direct Method INPUT]: Unloaded straight beam **b) [Direct Method OUTPUT]: Loaded bended beam**

Fig. 3 Direct method beam problem.

[Eq. (34)] and the Jacobian $J_0^{1(e)}$ [Eq. (35)], we need to compute the deformation gradient $\boldsymbol{F}_{\text{ref}}^{\mathbf{0}(e)}$ from the reference element Ω_{ref} to the undeformed element $\Omega^{\mathbf{0}(e)}$. Using the isoparametric mapping [see Eqs. (27–29)] equations:

$$\boldsymbol{x}^{\mathbf{0}(e)} = \boldsymbol{N}^{\text{ref}}(\boldsymbol{\xi}^{\text{ref}}) \cdot \hat{\boldsymbol{x}}^{\mathbf{0}(e)} \tag{38}$$

$$\boldsymbol{F}_{\text{ref}}^{\mathbf{0}(e)} = \left[\frac{\partial \boldsymbol{x}^{\mathbf{0}(e)}}{\partial \boldsymbol{\xi}^{\text{ref}}}\right] = \left[\frac{\partial \boldsymbol{N}^{\text{ref}} \cdot \hat{\boldsymbol{x}}^{\mathbf{0}(e)}}{\partial \boldsymbol{\xi}^{\text{ref}}}\right] = [\hat{\boldsymbol{x}}^{\mathbf{0}(e)}]^T \cdot \left[\frac{\partial \boldsymbol{N}^{\text{ref}}}{\partial \boldsymbol{\xi}^{\text{ref}}}\right] \tag{39}$$

$$J_{\text{ref}}^{\mathbf{0}(e)} = \det(\boldsymbol{F}_{\text{ref}}^{\mathbf{0}(e)}) \tag{40}$$

it is clear that all of these required quantities can be computed from the state of undeformed nodal positions $\hat{\boldsymbol{x}}^{\mathbf{0}}$.

From Eq. (37), it follows that the equilibrium equations (where the residue vanishes) are of the form:

$$\mathbf{R}\,(\hat{\boldsymbol{x}}^{\mathbf{1}}; \hat{\boldsymbol{x}}^{0}) = \mathbf{0} \tag{41}$$

with $\mathbf{R}$ given by Eq. (32).

In the next section, we will make use of the resulting general Eqs. (32) and (41) to present a unified approach for inverse design and standard direct methods.

IV. Inverse and Direct Methods in a Unified Approach

A. Standard Direct Method

In the standard direct method, the initial undeformed configuration of the structure is specified, i.e., $\hat{\boldsymbol{x}}^{\mathbf{0}} = \hat{\boldsymbol{x}}^{\mathbf{0}\text{input}}$ is given, and we want to determine how much the structure will deform when certain external loads are applied, i.e., we want to find the deformed state $\hat{\boldsymbol{x}}^{\mathbf{1}} = \hat{\boldsymbol{x}}^{\mathbf{1}\text{sol}}$ that satisfies the residual Eq. (41) with $\mathbf{R}$ given by Eq. (32):

$$\mathbf{R}\,(\hat{\boldsymbol{x}}^{\mathbf{1}\text{sol}}; \hat{\boldsymbol{x}}^{\mathbf{0}\text{input}}) = \mathbf{0} \tag{42}$$

Because $\hat{\boldsymbol{x}}^{\mathbf{0}\text{input}}$ is given, Eq. (42) is of the type

$$\mathbf{R}\,(\hat{\boldsymbol{x}}^{\mathbf{1}\text{sol}}) = 0 \tag{43}$$

and it can be solved iteratively using Newton–Raphson Method. At each iteration (k) we have to solve the linear system for the increment $\triangle\hat{\boldsymbol{x}}^{\mathbf{1}(k+1)}$

$$\mathbb{K}^{\mathbf{1}}(\hat{\boldsymbol{x}}^{\mathbf{1}(k)}) \cdot \triangle\hat{\boldsymbol{x}}^{\mathbf{1}(k+1)} = -\mathbf{R}\,(\hat{\boldsymbol{x}}^{\mathbf{1}(k)}, \hat{\boldsymbol{x}}^{\mathbf{0}\text{input}}) \tag{44}$$

where $\mathbb{K}^{\mathbf{1}}$ denotes the tangent matrix, given by

$$\mathbb{K}^{\mathbf{1}}(\hat{\boldsymbol{x}}^{\mathbf{1}}) = \frac{\partial \mathbf{R}(\hat{\boldsymbol{x}}^{\mathbf{1}}, \hat{\boldsymbol{x}}^{\mathbf{0}\text{input}})}{\partial \hat{\boldsymbol{x}}^{\mathbf{1}}} \tag{45}$$

Note that at $k = 0$ we choose $\hat{\boldsymbol{x}}^{\mathbf{1}(0)} = \hat{\boldsymbol{x}}^{\mathbf{0}\text{input}}$.

B. Inverse Design Method

In the inverse method discussed in this article one specifies the deformed body configuration $\mathcal{B}_h^{\mathbf{1}}$ and the problem is to find the corresponding unloaded (undeformed) geometry $\mathcal{B}_h^{\mathbf{0}}$. Mathematically speaking, this means that, now, the deformed configuration of the structure is specified, i.e., $\hat{\boldsymbol{x}}^{\mathbf{1}} = \hat{\boldsymbol{x}}^{\mathbf{1}\text{input}}$ is given, and we want to find the undeformed state $\hat{\boldsymbol{x}}^{\mathbf{0}} = \hat{\boldsymbol{x}}^{\mathbf{0}\text{sol}}$ that satisfies the residual Eq. (41) with $\mathbf{R}$ given by Eq. (32):

$$\mathbf{R}\,(\hat{\boldsymbol{x}}^{\mathbf{1}\text{input}}; \hat{\boldsymbol{x}}^{\mathbf{0}\text{sol}}) = \mathbf{0} \tag{46}$$

Because $\hat{\boldsymbol{x}}^{\mathbf{1}\text{input}}$ is given, Eq. (46) is of the type:

$$\mathbf{R}\,(\hat{\boldsymbol{x}}^{\mathbf{0}\text{sol}}) = 0 \tag{47}$$

and it can be solved iteratively using again the Newton–Raphson method employed in the direct method. At each iteration (k) we have to solve the linear system for the increment $\triangle\hat{\boldsymbol{x}}^{\mathbf{0}(k+1)}$

$$\mathbb{K}^{\mathbf{0}}(\hat{\boldsymbol{x}}^{\mathbf{0}(k)}) \cdot \triangle\hat{\boldsymbol{x}}^{\mathbf{0}(k+1)} = -\mathbf{R}\,(\hat{\boldsymbol{x}}^{\mathbf{1}\text{input}}, \hat{\boldsymbol{x}}^{\mathbf{0}(k)}) \tag{48}$$

where $\mathbb{K}^{\mathbf{0}}$ denotes the tangent matrix, given by

$$\mathbb{K}^{\mathbf{0}}(\hat{\boldsymbol{x}}^{\mathbf{0}}) = \frac{\partial \mathbf{R}(\hat{\boldsymbol{x}}^{\mathbf{1}\text{input}}, \hat{\boldsymbol{x}}^{\mathbf{0}})}{\partial \hat{\boldsymbol{x}}^{\mathbf{0}}} \tag{49}$$

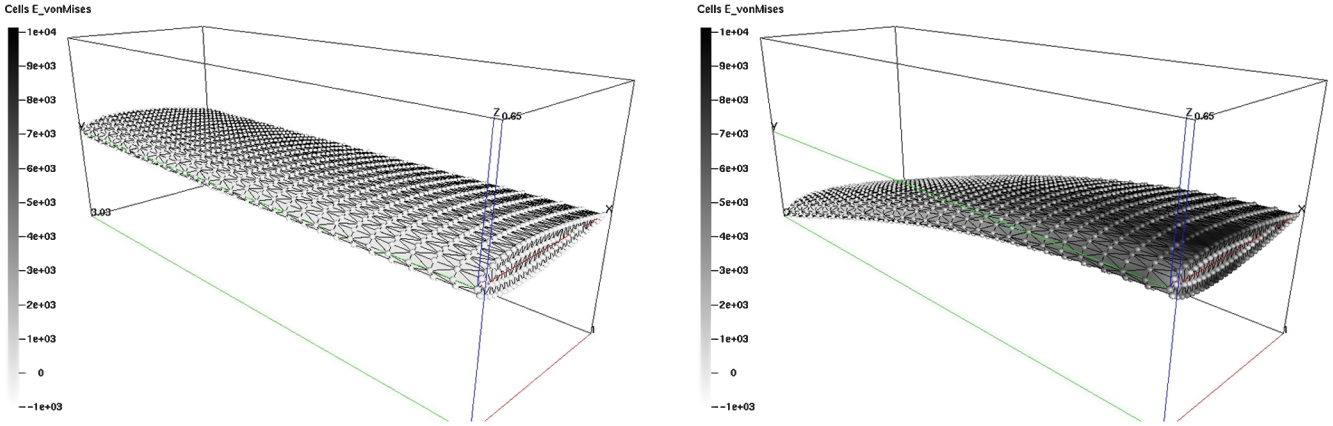
Note that at $k = 0$ we choose $\hat{\boldsymbol{x}}^{\mathbf{0}(0)} = \hat{\boldsymbol{x}}^{\mathbf{1}\text{input}}$.

Then, finding the inverse solution is as simple and natural as finding the solution of a direct problem. Actually, the residual function to be solved in the inverse problem is the same than the employed to solve the direct problem. The only difference, between the direct and the inverse problem, is that the tangent matrices are different. The tangent matrix of the inverse problem, $\mathbb{K}^{\mathbf{0}}$, can be computed either numerically or analytically in the same way the tangent matrix for the direct problem is computed. In the next sections, numerical results are presented.

V. Numerical Solutions

The direct/inverse method described above have been implemented in the `MulPhys` code[†] [24]. The duality presented in the mathematical formulation allows the user to change from direct analysis to inverse design, quickly and easily. In this section, we present some interesting numerical solutions obtained using the program. First, we will consider the standard direct approach in Sec. V.A, and after that, we will consider the inverse problem in Sec. V.B.

[†]MulPhys is a tool for multiphysics by computers; data available online at http://www.cimec.org.ar/alimache/ [retrieved July 2010].



a) [Direct Method INPUT]: Unloaded straight wing b) [Direct Method OUTPUT]: Loaded bended wing

Fig. 4 Direct method wing problem.

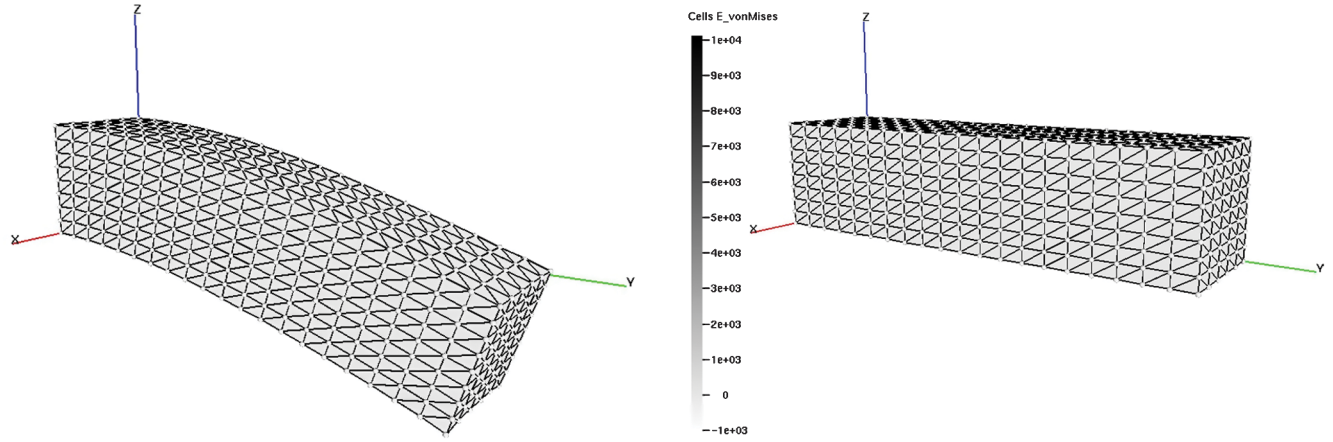
A. Direct Method

Let us consider two examples. In all cases SI units are used. The first example consists of a perfectly rectangular beam made of an hyperelastic material whose constitutive equation is given by

$$\boldsymbol{S}_{\boldsymbol{0}}^{\boldsymbol{1}} = \mathbb{C} \cdot \boldsymbol{E}_{\boldsymbol{0}}^{\boldsymbol{1}} \tag{50}$$

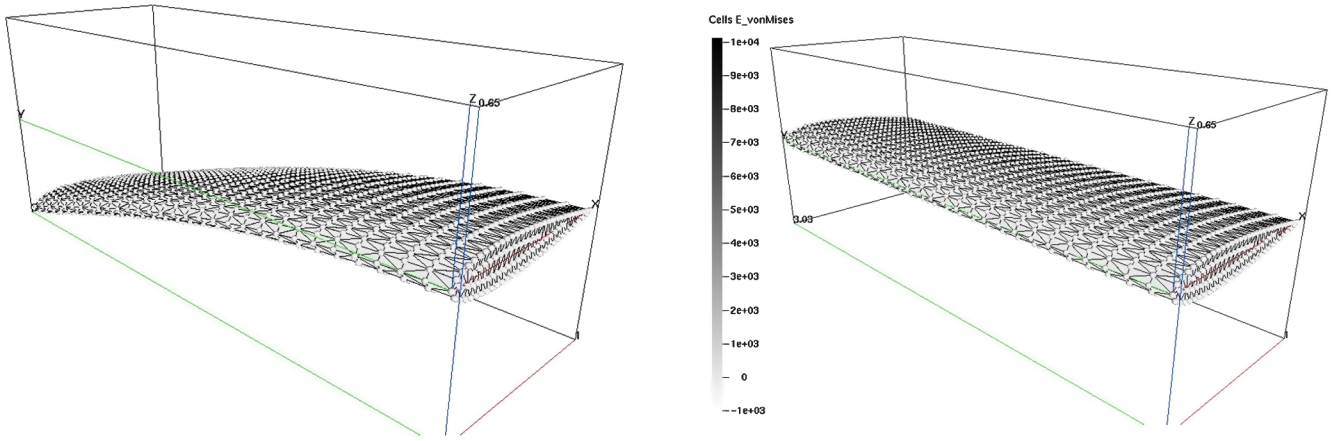
where $\mathbb{C}$ is the fourth order isotropic material tensor [25], having a Young's module $E = 2 * 10^5$, a Poisson ratio $\nu = 0.3$, and a density $\rho^{\boldsymbol{0}} = 1.0$.

The bar has a squared section of sides $S = 1.0$ and lenght $L = 4.0$. It is clamped to the wall on its left side as Fig. 3a, shows. The flexible beam is loaded with two nodal forces acting downward on the lower corners of the right side. In the direct method case, given these



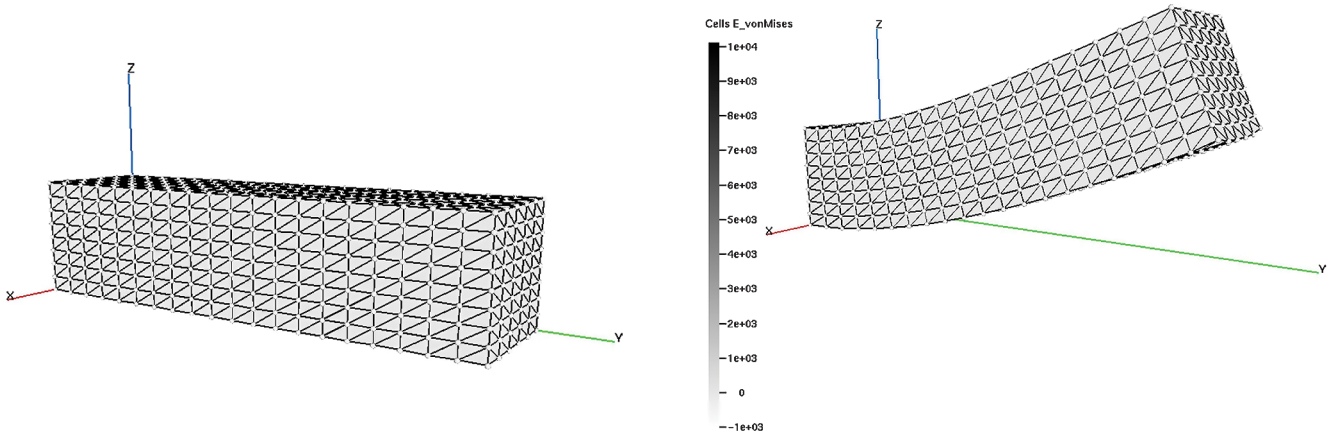
a) [Inverse Method INPUT]: loaded downwards bended beam b) [Inverse Method OUTPUT]: Unloaded rectangular beam

Fig. 5 Inverse method beam test problem.



a) [Inverse Method INPUT]: Loaded downwards bended wing b) [Inverse Method OUTPUT]: Unloaded straight wing

Fig. 6 Inverse method wing test problem.



a) [Inverse Method INPUT]: Loaded straight beam

b) [Inverse Method OUTPUT]: Unloaded upwards-bended designed beam

Fig. 7 Inverse method beam design problem.

imposed loads applied over the undeformed beam, the problem consists in determining the resulting deformation of the beam. The numerical results for this particular direct problem are shown in Fig. 3b. Because of the downside external forces the flexible beam curves down having a deflection at the tip of $\delta = -0.93$. Figures 3a and 3b also show the given initial (zero) von-Mises stresses and the final von-Mises stresses predicted by the numerical simulation, respectively.

The second test is the case of an airplane wing formed with NACA 0012 airfoils of chord $c = 1.0$ and a wing span of $b = 5.0$, as shown in Fig. 4a. The wing was made of the same hyperelastic material given in Eq. (50), having a Young's module $E = 2 * 10^6$, a Poisson ratio $\nu = 0.3$, and a density $\rho^{\mathbf{0}} = 1.0$. To simulate the application of aerodynamic forces the wing was assumed to be clamped at the fuselage (right side of the half-wing shown in Fig. 4a) and loaded with downside external forces acting on the wing's left tip. The direct problem consists in determining what will be the resulting deformation of the wing as a consequence of its own weight and the imposed loads. The results are shown in Fig. 4b. As shown in these figures, because of the downside external forces, the flexible wing bends downwards along its left tip. Figures 4a and 4b also show the initial (zero) von-Mises stresses and the final von-Mises stresses predicted by the numerical simulation, respectively.

B. Inverse Method: Validation Tests

In the inverse method, one specifies the desired deformed configuration for given loads and the problem becomes to determine the corresponding unloaded/undeformed geometry of such structure. Here, we will validate the inverse design method by checking that when the loaded configurations computed in Sec. V.A (i.e., Figs. 3b and 4b) are given as inputs to the inverse program, the outputs are the corresponding initial undeformed structures (i.e., Figs. 3a and 4a).

The numerical results for these validation tests cases are shown in Figs. 5 and 6. Figure 5b shows how the straight bar defined in Fig. 3a is recovered when the loaded structure is supplied (Fig. 5a). Figure 6b shows how the rectilinear wing defined in Fig. 4a is recovered when the deformed wing structure is supplied (Fig. 6a). As can be seen from the figures the method works successfully.

C. Inverse Method: Design Cases

In practical manufacturing processes, usually, one wants to have structures that once loaded and deformed by known external forces acquire predefined ideal shapes. Here, two interesting and practical design cases derived from the examples discussed above are presented.

Consider first the case of manufacturing a beam of a desired shape. Ideally, a civil engineer would like to work with a nonbended clamped beam, having a perfectly straight rectangular shape, like the one shown in Fig. 3a. He can not simply request to manufacture such rectilinear beam, because once loaded, the initially perfectly straight beam will deform acquiring a bended shape like the one shown in Fig. 3b. He faces then the following problem: what would have to be the undeformed configuration of the clamped beam that needs to be manufactured, so as to when loaded with specific external forces, it will acquire the form of a perfectly rectangular structure? Using the inverse method presented in this paper, one can easily determine such shape. The procedure is simple. Provide, as INPUT, the desired deformed shape with the specific external forces. In our case, the desired shape is the rectangular beam shown in Fig. 7a. The OUTPUT of the Inverse method will determine what is the actual shape of the beam that needs to be manufactured. In our case the computed shape is shown in Fig. 7b.

A direct method evaluation of the upward-bended beam shown in Fig. 7b proves that in fact when such beam is loaded with the input downside external forces, it actually deforms acquiring a perfectly straight rectangular shape. In Fig. 8 the results of the evaluation are shown, with the loaded beam becoming rectangular. The figure also shows the resulting distribution of stresses.

As a final example, consider a structural wing design problem. Suppose that an aeronautical engineer wants to use a constant chord rectilinear wing with perfect NACA 0012 wing sections because such wing's geometry has some very desirable aerodynamic characteristics. He can not simply manufacture this ideal wing (shown in Fig. 4a), because its weight and the strong aerodynamic forces acting on the desired flight conditions will bend or twist it, resulting in an undesirable deformed shape like, for example, the one shown in Fig. 4b. He faces then the following problem: what would have to be the initial wing geometry that needs to be manufactured, so as to when flying under the influence of the aerodynamic loads, the wing will acquire a perfectly rectilinear form with constant chord

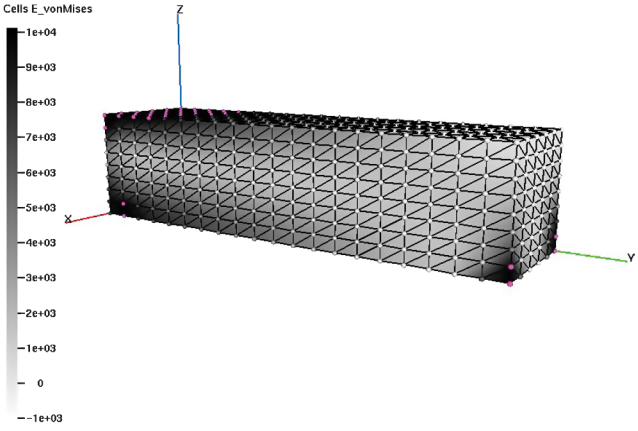
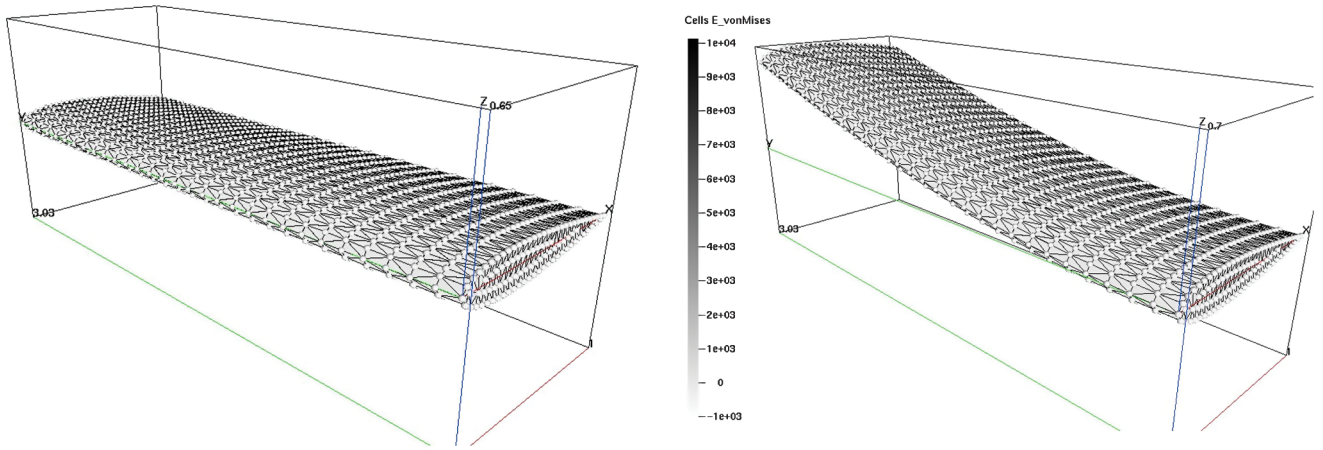


Fig. 8 Testing the inverse designed beam.



a) [Inverse Method INPUT]: Loaded straight wing

b) [Inverse Method OUTPUT]: Unloaded upwards-bended designed wing

Fig. 9 Inverse method wing design problem.

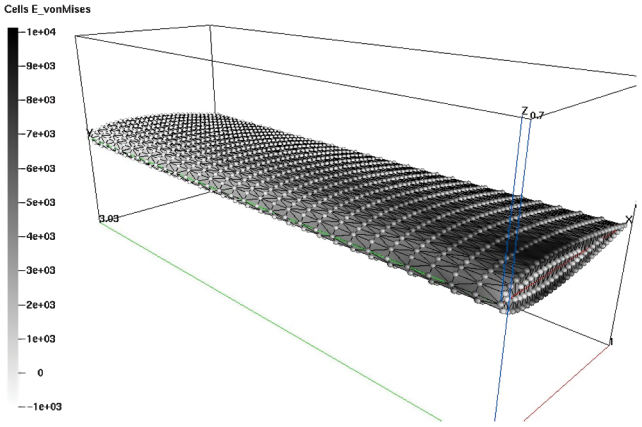


Fig. 10 Testing the inverse designed wing.

NACA 0012 wing sections? Using the inverse method presented in this paper, one can easily determine such initial shape. The procedure is simple. Provide, as INPUT, the desired wing shape together with the acting loads. In our case, the desired shape is the straight wing shown in Fig. 9a. The OUTPUT of the Inverse method will determine what is the actual wing shape that needs to be manufactured. In our case the computed OUTPUT shape is shown in Fig. 9b. A direct method evaluation of the designed upward-bended wing shown in Fig. 9b proves that in fact when such wing gets loaded with the input downside forces and its own weight, it actually deforms acquiring the configuration of a perfectly straight wing, as it is shown in Fig. 10. Figure 10 also shows the resulting distribution of stresses at such deformed configuration.

VI. Conclusions

A general inverse method for the shape design of deformable structures has been presented. The method can determine the initial shape of structures such when deformed will acquire specifically desired target configurations. The method is based on a novel mathematical formulation that exploits a duality concept between deformed and undeformed states. One of the major advantages of the presented method, is that it can be easily implemented on top of the machinery of standard direct method programs. In particular, it does not need a new residual evaluation routine, it just makes use of the standard residue's subroutine of the direct problem. General continuum mechanics has been incorporated to the formulation, so the method is not restricted to the small perturbations or linear elasticity theory and can handle large deformable structural design. The method is a extremely promising tool for multiple engineering areas and manufacturing processes. In this article examples have been presented oriented to the shape design of beams and airplane wings.

Acknowledgments

Financial support by Consejo Nacional de Investigaciones Científicas y Técnicas and by Agencia Nacional de Promoción Científica y Tecnológica is gratefully acknowledged.

References

[1] Limache, A. C., and Idelsohn, S. R., "On the Development of Finite Volume Methods for Computational Solid Mechanics," *Mecánica Computacional*, Vol. 26, No. 11, 2007, pp. 827–843.

[2] Limache, A. C., and Cliff, E. M., "Aerodynamic Sensitivity Theory for Rotary Stability Derivatives," *Journal of Aircraft*, Vol. 37, No. 4, 2000, pp. 676–683. doi:10.2514/2.2651

[3] Anderson, W. K., and Ventakakrishnan, V., "Aerodynamic Design Optimization on Unstructured Grids with a Continuous Adjoint Formulation," AIAA 97–0643, 1997.

[4] Maruyama, D., Matsushima, K., Kusunose, K., and, Nakahashi, K., "Three-Dimensional Aerodynamic Design of Low-Wave-Drag Supersonic Biplane Using Inverse Problem Method," *Journal of Aircraft*, Vol. 46, No. 6, 2009, pp. 1906–1918. doi:10.2514/1.40313

[5] Wu, L., Shields, E., and Le, D., "Interactive Inverse Design Optimization of Fuselage Shape for Low-Boom Supersonic Concepts," *Journal of Aircraft*, Vol. 45, No. 4, 2008, pp. 1381–1397. doi:10.2514/1.35543

[6] Barrett, T., Bressloff, N., and Keane, A. J., "Airfoil Shape Design and Optimization Using Multifidelity Analysis and Embedded Inverse Design," *AIAA Journal*, Vol. 44, No. 9, 2006, pp. 2051–2060. doi:10.2514/1.18766

[7] Qin, N., Vavalle, A., Le Moigne, A., Laban, M., Hackett, K., and Weinerfelt, P., "Aerodynamic Considerations of Blended Wing Body Aircraft," *Progress in Aerospace Sciences*, Vol. 40, No. 6, 2004, pp. 321–343. doi:10.1016/j.paerosci.2004.08.001

[8] Lepine, J., Guibault, F., Trepanier, J., and Pepin, F., "Optimized Nonuniform Rational *B*-spline Geometrical Representation for Aerodynamic Design of Wings," *AIAA Journal*, Vol. 39, No. 11, 2001, pp. 2033–2041. doi:10.2514/2.1206

[9] Ahn, T., Kim, H., Kim, C., and Oh-Hyun, R., "Inverse Design of Transonic Wings Using Wing Planform and Target Pressure Optimization," *Journal of Aircraft*, Vol. 38, No. 4, 2001, pp. 644–652. doi:10.2514/2.2841

[10] Limache, A. C., "An Inverse Method for Airfoil Design," *Journal of Aircraft*, Vol. 32, No. 5, 1995, pp. 1001–1011. doi:10.2514/3.46829

[11] Limache, A. C., "Hodograph Method for Airfoil Design: The General

Case," *Journal of Aircraft*, Vol. 33, No. 4, 1996, pp. 680–690. doi:10.2514/3.47002

[12] Takanashi, S., "Iterative Three Dimensional Transonic Wing Design Using Integral Equations," *Journal of Aircraft*, Vol. 22, No. 8, 1985, pp. 655–660. doi:10.2514/3.45182

[13] Liu, G., "A New Generation of Inverse Shape Design Problem in Aerodynamics and Aerothermoelasticity: Concepts, Theory and Methods," *Aircraft Engineering and Aerospace Technology*, Vol. 72, No. 4, 2000, pp. 334–344.

[14] Pawar, P. M., and Ganguli, R., "Genetic Fuzzy System for Damage Detection in Beams and Helicopter Rotor Blades," *Computer Methods in Applied Mechanics and Engineering*, Vol. 192, Nos. 16–18, 2003, pp. 2031–2057. doi:10.1016/S0045-7825(03)00237-8

[15] Chandrashekhar, M., and Ganguli, R., "Structural Damage Detection Using Modal Curvature and Fuzzy Logic," *Structural Health Monitoring*, Vol. 8, 2009, pp. 267–282. doi:10.1177/1475921708102088

[16] Farrar, C., Doebling, S., and Nix, D., "Structural Damage Detection Using Modal Curvature and Fuzzy Logic," *Philosophical Transactions of the Royal Society of London, Series A: Mathematical and Physical Sciences*, Vol. 359, No. 1778, 2001, pp. 131–149. doi:10.1098/rsta.2000.0717

[17] Govindjee, S., and Mihalic, P. A., "Computational methods for inverse finite elastostatics," *Computer Methods in Applied Mechanics and Engineering*, Vol. 136, Nos. 1–2, 1996, pp. 47–57. doi:10.1016/0045-7825(96)01045-6

[18] Govindjee, S., and Mihalic, P. A., "Computational Methods for Inverse Deformations in Quasi-Incompressible Finite Elasticity," *International Journal for Numerical Methods in Engineering*, Vol. 43, No. 5, 1998, pp. 821–838. doi:10.1002/(SICI)1097-0207(19981115)43:5<821::AID-NME453>3.0.CO;2-C

[19] Yamada, T., "Finite Element Procedure of Initial Shape Determination for Hyperelasticity," *Structural Engineering and Mechanics*, Vol. 6, No. 2, 1998, pp. 173–183.

[20] Fachinotti, V. D., Cardona, A., and Jetteur, P., "Finite Element Modelling of Inverse Design Problems in Large Deformations Anisotropic Hyperelasticity." *International Journal for Numerical Methods in Engineering*, Vol. 74, No. 6, 2008, pp. 894–910. doi:10.1002/nme.2193

[21] Ogden, R. W., *Elastic Deformations*, Series in Mathematics and its Applications, Ellis Horwood Limited, London, 1984.

[22] Oñate, E., *Calculo de Estructuras por el Método de Elementos Finitos*, International Center for Numerical Methods in Engineering, Barcelona, 1995.

[23] Johnson, C., *Numerical Solution of Partial Differential Equations by the Finite Element Method*, Cambridge Univ. Press, Cambridge, England, 1995.

[24] Alves de Queiroz, T., and Limache, A. C., "Evaluation of Numerical Algorithms for Non-Linear Solid Mechanics," *Proceedings of the 6th Brazilian Conference on Dynamics, Control and Their Applications*, 2007.

[25] Ottosen, N., and Ristinmaa, M., *The Mechanics of Constitutive Modeling*, Elsevier, New York, 2005.